Liu et al. *Zool. Res.* 2025, 46(2): 313−324
https://doi.org/10.24272/j.issn.2095-8137.2024.229
https://cstr.cn/32248.14.zr.2024.229

ZR | Zoological Research

Article Open Access

Knockout of the *fcsk* gene in zebrafish causes neurodevelopmental defects

Zhen-Xing Liu[1,#], Ting-Ting Zou[1,#], Hui-Hui Liu[1], Hai-Bo Jia[1,*], Xian-Qin Zhang[1,*]

[1] *Key Laboratory of Molecular Biophysics of the Ministry of Education*, *College of Life Science and Technology and Center for Human Genome Research*, *Huazhong University of Science and Technology*, *Wuhan*, *Hubei* 430074, *China*

ABSTRACT

Congenital disorders of glycosylation (CDG) are a cluster of monogenic disorders resulting from defects in glycosylation. *FCSK* encodes fucokinase, an enzyme that catalyzes the phosphorylation of L-fucose to generate fucose-1-phosphate, an important step in fucosylation. Mutations in *FCSK* lead to CDG with an autosomal recessive inheritance pattern, primarily manifesting as developmental delay, hypotonia, and brain abnormalities. However, no *fcsk* mutant animal models have yet been established. This study constructed the first *fcsk* knockout (*fcsk*$^{-/-}$) zebrafish model using CRISPR/Cas9 technology. Notably, *fcsk*$^{-/-}$ zebrafish exhibited impaired growth, characterized by delayed epiboly and DNA accumulation during early embryonic development, as well as brain atrophy in adulthood. Larval-stage *fcsk*$^{-/-}$ zebrafish displayed locomotor deficits and increased susceptibility to pentylenetetrazole-induced seizures. In adulthood, *fcsk*$^{-/-}$ zebrafish showed neurodevelopmental abnormalities, including increased anxiety, decreased aggression, reduced social preference, and impaired memory. Additionally, total protein fucosylation was markedly reduced in *fcsk*$^{-/-}$ zebrafish, accompanied by decreased expression of *pofut2*, which encodes protein O-fucosyltransferase 2, an enzyme involved in the fucosylation salvage pathway. Apoptotic activity was elevated in the midbrain-hindbrain boundary (MHB) of *fcsk*$^{-/-}$ zebrafish. Supplementation with GDP-L-fucose or the human *FCSK* gene restored developmental defects and total protein fucosylation in *fcsk*$^{-/-}$ zebrafish. RNA sequencing revealed dysregulated gene expression associated with glycosylation, apoptosis, and neurodegenerative diseases. These findings suggest that *fcsk*$^{-/-}$ zebrafish exhibit neurodevelopmental disorders, providing the first *fcsk* gene knockout animal model and offering a platform for investigating the molecular underpinnings of the disease and facilitating drug screening efforts.

Keywords: Congenital disorders of glycosylation; *fcsk*; Zebrafish; Behavior; RNA sequencing

INTRODUCTION

Congenital disorders of glycosylation (CDG) represent a diverse group of genetic diseases arising from defects in protein and lipid glycosylation, affecting key glycosylation pathways and exhibiting substantial phenotypic and genetic heterogeneity (Ng & Freeze, 2018; Ondruskova et al., 2021). To date, more than 150 pathogenic genes associated with CDG have been identified (Ondruskova et al., 2021). Based on the function of the affected genes, CDG can be classified into disorders related to N-linked glycosylation, O-linked glycosylation, glycosylphosphatidylinositol (GPI) anchor biosynthesis, and multiple glycosylation pathways (Hüllen et al., 2021; Ondruskova et al., 2021). The latter category includes defects in monosaccharide synthesis and interconversion, Golgi pH and ion homeostasis, and vesicular trafficking, among other processes (Hüllen et al., 2021; Ondruskova et al., 2021). The FCSK protein is responsible for the phosphorylation of β-L-fucopyranose in the salvage pathway of GDP-fucose biosynthesis. CDG resulting from *FCSK* deficiency is classified as a monosaccharide synthesis and interconversion disorder (Ondruskova et al., 2021). At present, five genes are known to cause CDG due to fucose deficiency, including *FUK*, *FUT8*, *POFUT1*, *SLC35C1*, and *GFUS* (Feichtinger et al., 2021). L-fucose supplementation has been shown to partially ameliorate symptoms in individuals with fucose-related CDG (Feichtinger et al., 2021; Hüllen et al., 2021). *Aleuria aurantia* lectin (AAL), a plant-

Received: 31 October 2024; Accepted: 26 November 2024; Online: 27 November 2024

Foundation items: This work was supported by the National Key R&D Program of China (2023YFC2706302), National Natural Science Foundation of China (81000079, 81170165 and 81870959 to X.Z.), Program of HUST Academic Frontier Youth Team (2016QYTD02), and Fundamental Research Funds for the Central Universities (HUST: 2019JYCXJJ035)

[#]Authors contributed equally to this work

*Corresponding authors, E-mail: xqzhang04@hust.edu.cn; haibo.jia@hust.edu.cn

derived lectin, selectively binds to fucose-containing glycoconjugates, such as fucosylated proteins and lipids, making it a valuable tool for detecting fucosylation abnormalities (Taubenschmid et al., 2017).

De novo and salvage synthesis pathways represent crucial sources of GDP-fucose in mammals (Feichtinger et al., 2021; Hüllen et al., 2021). To investigate the molecular basis of CDG caused by fucose metabolism defects, zebrafish and mouse models deficient in *FUT8*, *POFUT1*, *SLC35C1*, and *GFUS* have been developed (Hayashiji et al., 2022; Li et al., 2013; Smith et al., 2002; Yakubenia et al., 2008). *FUT8* and *POFUT1* encode fucosyltransferases responsible for allocating sugar residues of GDP-L-fucose to N-glycans and O-glycans, respectively (Hayashiji et al., 2022; Li et al., 2013). Patients with *FUT8* mutations exhibit developmental delay, hypotonia, facial dysmorphism, respiratory failure, neurological impairment, and swallowing difficulties (Ng et al., 2018b; Wang et al., 2005). Knockdown of *fut8a* in zebrafish results in delayed development, defective myotome formation, and dorsal deformities (Hayashiji et al., 2022). Mutations in *POFUT1* underlie Dowling-Degos disease, a pigmentary disorder characterized by reticulate hyperpigmentation in flexural areas or hypopigmentation (Li et al., 2013). Knockdown of *pofut1* in zebrafish leads to hypopigmentation at 48 hours post-fertilization (hpf) and disrupted melanin distribution at 72 hpf (Li et al., 2013). Despite the availability of animal models for other fucosylation-related genes, no animal model has been established for *FCSK* deficiency. To address this gap, a zebrafish model with *fcsk* (human *FCSK* ortholog) deletion was constructed to investigate pathogenic mechanisms. *FCSK* (also known as *FUK*) encodes fucokinase, a key enzyme in the GDP-fucose salvage pathway (Feichtinger et al., 2021; Hüllen et al., 2021). Mutations in *FCSK* result in CDG, manifesting as developmental delay, hypotonia, brain and ocular abnormalities, seizures, feeding difficulties, bone contractures, and respiratory dysfunction (Al Tuwaijri et al., 2023; Manoochehri et al., 2022; Ng et al., 2018a; Özgün & Şahin, 2022). To date, only four studies have reported *FCSK* mutations causing CDG, all involving loss-of-function variants that disrupt the fucose salvage pathway (Al Tuwaijri et al., 2023; Manoochehri et al., 2022; Ng et al., 2018a; Özgün & Şahin, 2022). However, the mutation spectrum and associated clinical features remain poorly characterized, and effective treatment options are lacking. Human FCSK and zebrafish Fcsk proteins share a high degree of amino acid sequence homology, making zebrafish a suitable model for studying the molecular mechanisms underlying *FCSK*-related CDG. A well-characterized *fcsk*-deficient animal model is crucial for replicating CDG phenotypes, elucidating disease mechanisms, and identifying potential therapeutic targets.

In this study, an *fcsk*-knockout zebrafish model was generated, and its phenotype, glycosylated protein expression, and transcriptomic alterations were systematically analyzed. This model provides a comprehensive framework for understanding the developmental and molecular pathophysiology of CDG, spanning embryogenesis to adulthood, offering valuable insights into disease progression and potential therapeutic interventions.

MATERIALS AND METHODS

Zebrafish maintenance

Wild-type (WT) AB strain zebrafish were purchased from the Institute of Hydrobiology, Chinese Academy of Sciences, and cultured in a recirculating water system at 28.5°C under a 14 h light and 10 h dark cycle. The night before spawning, healthy, sexually mature zebrafish (male-to-female ratio of 2:1) were placed in designated breeding tanks. Fertilized eggs were collected the following morning, washed three times with embryo culture water, and incubated at 28.5°C for further development. Larvae from 0 to 5 days post-fertilization (dpf) were maintained in an incubator, with embryo water changed twice daily and non-viable embryos removed promptly. Larvae from 5 to 15 dpf were cultured in small tanks and fed paramecia twice daily. From 10 dpf, zebrafish were supplemented with brine shrimp, and one-third of the tank water was replaced daily. After 15 dpf, the zebrafish were fed brine shrimp twice daily. Upon reaching 30 dpf, zebrafish were transferred to a recirculating water system for further cultivation. For experimental procedures, zebrafish embryos and larvae were anaesthetized with tricaine (Macklin, China), while adult zebrafish were euthanized via ice immersion. Adult zebrafish body length was measured from the anterior-most point of the head to the end of the tail using a ruler.

Ethics approval

All applicable international, national, and/or institutional guidelines for the care and use of animals were strictly followed. All animal sample collection protocols complied with the current laws of China. All animal procedures performed in this research were reviewed and approved by the Ethics Committee of Huazhong University of Science and Technology, Wuhan, China ([2021] IACUC Number: 3083).

Construction of *fcsk* mutant zebrafish using CRISPR/Cas9

The target gRNA (5'-CCATGGGACGGGTTTTCTGGGGT-3') for zebrafish *fcsk* (GRCz11: CM002909.2) knockout was designed using CHOPCHOP (http://chopchop.cbu.uib.no/). The gRNA sequence, T7 promoter, and gRNA scaffold were amplified via polymerase chain reaction (PCR) using the PMD19-T plasmid as a template. The amplified product was then transcribed into RNA *in vitro* using the Transcript Aid T7 High Yield Transcription Kit (Thermo Fisher, USA). The gRNA (1 000 ng/μL) and Cas9 protein (500 ng/μL; EASTINNO, China) were mixed at a 1:1 ratio, and approximately 8 nL of the mixture was injected into one- to two-cell-stage WT embryos. Genotyping of WT and *fcsk* mutant zebrafish was performed using either Sanger sequencing (forward primer ACATTAATGCACAAACTCAACACTG and reverse primer AATGTTGCGCACTCTGGTCT) or enzyme digestion (NcoI endonuclease).

Sanger sequencing revealed overlapping chromatogram peaks near the gRNA recognition site, indicating effective knockout (defined as the F_0 generation). F_0 zebrafish were mated with WT zebrafish to generate the F_1 generation, and genotyping of F_1 progeny identified three distinct mutations, including c.160_164delTGGGA, c.164_168delACGGG, and c.163_164delGA. Among these, only the c.160_164del TGGGA mutation was present in both female and male zebrafish. Therefore, this study mainly focused on c.160_164delTGGGA mutant zebrafish. F_1 heterozygous zebrafish carrying the c.160_164delTGGGA mutation were intercrossed to obtain F_2 generation homozygous zebrafish (c.160_164delTGGGA), which were further intercrossed to establish the F_3 generation. Homozygous F_2 and F_3 zebrafish were used for subsequent phenotypic and molecular analyses.

Semi-quantitative RT-PCR and reverse transcription-quantitative real-time PCR (RT-qPCR)

Total RNA was extracted from zebrafish embryos or tissues using TRIzol reagent (Takara, Japan) and crushed using a homogenizer (Bertin Precellys Evolution, France). Total RNA was precipitated through organic solvents, chloroform and isopropanol, and washed twice with 75% ethanol. Reverse transcription was performed using a HiScript 1st-Strand cDNA Synthesis Kit (Vazyme, China). PCR amplification products were detected by agarose gel electrophoresis and visualized using the Bio-Rad XR+ gel documentation system (USA). Semi-quantitative analysis was conducted using Image Lab v.5.0 software. For RT-qPCR, reactions were performed using Hieff® qPCR SYBR Green Master Mix (Yeasen, China) on an Applied Biosystems™ QuantStudio™ 3 & 5 real-time PCR system (Thermo Fisher, USA). Primers were designed using Primer3 and BLAST (NCBI Primer-BLAST) against the zebrafish reference genome GRCz11 (*Danio rerio*). The following primers were used: *fcsk* forward GCTGAATA TTCCAACGCGACA and reverse CAGAGATATCTCAAG TGGTGG; *actb1* forward ACCACGGCCGAAAGAGAAAT and reverse ATGTCCACGTCGCACTTCAT; and *pofut2* forward GGATGTTCGCTACCTCCTGT and reverse CCATTACTGAC GTGGCTGTTATG.

DNA extraction

Genomic DNA was extracted from zebrafish embryos using the phenol-chloroform method (Zhao et al., 2017). DNA content was measured using a NanoDrop One spectrophotometer (Thermo Fisher, USA).

Light-dark stimulation test for zebrafish larvae

To assess locomotor responses to light-dark transitions, 6 dpf zebrafish larvae were individually placed into the wells of a 96-well plate. The plate was transferred to a zebrafish video tracker system (Noldus, Netherlands) and acclimated for 30 min. Subsequently, four alternating dark (5 min) and light (5 min) stimulations were performed. EthoVision XT7 (Noldus, Netherlands) was used for data analysis, and the raw data were transformed into total movement distance to quantify motion activity after stimulation.

Pentylenetetrazole (PTZ) stimulation test in zebrafish larvae

To assess seizure susceptibility, 6 dpf zebrafish larvae were individually placed in a 96-well plate and transferred to the Noldus zebrafish video tracking system (Netherlands) for behavioral monitoring. Larvae were acclimated under continuous light for 60 min, after which PTZ (Macklin, China) was added to a final concentration of 10 mmol/L. After a 10-min adaptation period, locomotor activity was recorded for 20 min. The cumulative duration of high-speed movements was quantified using a movement speed threshold of more than 20 mm/s.

Behavioral assays in adult zebrafish

Novel tank test: The novel tank test was conducted to assess fear and anxiety-like behavior based on exploratory activity in a new environment (Raymond et al., 2012). Increased time spent in the lower zone of the novel tank indicates heightened anxiety. WT and mutant zebrafish, age-matched at 3 mpf and reared under identical conditions, were individually placed in a 26 cm length×9 cm width×20 cm height tank filled with water to a depth of 18 cm. The tank was divided into three equal horizontal zones: lower, middle, and upper. Following 5 min of acclimation, zebrafish behavior was recorded for 6 min. Videos were analyzed using Noldus tracking software (EthoVision XT v.14.0.1314) to determine time spent in each region and total movement distance.

Mirror biting test: The mirror biting test was employed to assess aggression, as zebrafish perceive their reflection as a competitor and engage in attack behaviors (Raymond et al., 2012). WT and mutant zebrafish (3 mpf) reared under identical conditions were placed into a 29 cm length×9 cm width×15 cm height tank filled with water to a depth of 14 cm. The tank was divided into three behavioral zones: contact zone (0–2 cm from the mirror), approach zone (2–6 cm from the mirror), and far zone (>6 cm from the mirror). After 3 min of acclimation, zebrafish behavior was recorded for 6 min. Videos were analyzed using Noldus tracking software (EthoVision XT v.14.0.1314), measuring time spent in each zone and total distance traveled. Prolonged occupancy in the contact zone was interpreted as a sign of increased aggression.

Social preference test: The social preference test was conducted to evaluate zebrafish sociability by assessing their tendency to interact with conspecifics (Liu et al., 2018). WT and mutant zebrafish (3 mpf) raised under the same conditions were individually placed in a social preference apparatus (20 cm length×10 cm width×10 cm height) filled with water to a depth of 8 cm. The apparatus was divided into two sections by a transparent plate of plexiglass. Prior to testing, a stimulus group of three adult zebrafish was placed in the right compartment, with fresh zebrafish used for each trial to ensure active behavior. A test zebrafish was placed in the left compartment, separated by an opaque white barrier positioned in front of the transparent divider. Following 5 min of acclimation, the opaque barrier was removed, and behavior was recorded for 5 min. Time spent in each area and total movement distance were analyzed using Noldus tracking software (EthoVision XT v.14.0.1314).

Shoaling test: The shoaling test was used to assess the coordination and proximity of social behavior by quantifying inter-individual distances among freely swimming zebrafish groups (Liu et al., 2018). WT and mutant zebrafish (3 mpf) kept under the same conditions were introduced into a shoaling arena (40 cm length×40 cm width×20 cm height) filled with water to a depth of 18 cm. Six zebrafish of the same genotype were placed in the tank, allowed to acclimate for 5 min, and then recorded for 5 min. To quantify shoaling behavior, video frames were captured every 20 s, generating 15 frames per trial. Inter-fish distances were measured using Adobe Photoshop to determine group cohesion and shoaling tendencies.

Modified T-maze test: The modified T-maze test was used to assess learning and memory behaviors in zebrafish. The modified T-maze apparatus consisted of two deep-water arms and one long straight arm, forming a T-shape (Ngoc Hieu et al., 2020). The straight arm (300 mm length×80 mm width×60 mm height) was partitioned using a white panel to create a starting chamber, while the deep-water arms (100 mm length×100 mm width×100 mm height) served as choice zones. A green board was positioned inside the right deep-water arm to guide zebrafish (3 mpf) toward the left deep-water arm (punishment arm). On day 1, the zebrafish were allowed to freely explore the entire T-maze for 30 min to acclimate to the new environment. On day 2, electrical shocks (10 V and 0.3–0.5 mA) were administered to the left deep-water arm for punishment training. On day 3, testing was

conducted by recording the latency to enter the left deep-water arm, to evaluate memory retention.

Acridine orange (AO) staining

AO staining was used to detect apoptosis in WT and mutant embryos (30 hpf). Staining was conducted at 28.5°C for 30 min using an AO Staining Kit (Sangon Biotech, China). The stained embryos were then washed three times with ultrapure water and imaged using fluorescence microscopy (Nikon 80i, Japan).

Western and lectin blots

Total protein from 20 larvae (5 dpf) was extracted for western and lectin blot analyses. The zebrafish were placed in RIPA lysis buffer (Beyotime, China) containing a protease inhibitor (Roche, Germany), and mechanical lysis was performed using a homogenizer and ultrasound. After centrifugation at 15 000 ×*g* for 15 min at 4°C, the supernatant was collected, and SDS-PAGE loading buffer was added and denatured by heating at 100°C for 15 min. The proteins were then separated using 10% sodium dodecyl-sulfate polyacrylamide gel electrophoresis (SDS-PAGE) and transferred to polyvinylidene fluoride (PVDF) membranes. After incubation with TBS buffer containing 0.1% Tween-20 (TBST) for 1 h at room temperature, the PVDF membranes were exposed to biotinylated AAL (1:1 000 in TBST; Vector Laboratories, USA) and incubated overnight at 4°C. The lectin-binding proteins were detected using horseradish peroxidase (HRP)-conjugated streptavidin (1:10 000 in TBST; Proteintech, China). The chemiluminescent signal was captured using the ChemiDoc XRS+ System (Bio-Rad, USA).

Rescue experiments

Approximately 8 nL of GDP-L-fucose (30 mmol/L; Macklin, China) or GFP-tagged human *FCSK* gene expression vector (50 ng/μL) was injected into one- to two-cell-stage mutant embryos (*fcsk*$^{-/-}$) (Fowler et al., 2021). The control group was injected with water or empty vector. At 48 hpf or 5 dpf, the level of fucosylation was assessed, followed by measurement of zebrafish body length at 5 dpf.

RNA sequencing (RNA-seq)

Total RNA was extracted from 5 dpf larvae using TRIzol reagent, followed by mRNA enrichment using Oligo dT magnetic beads. Library construction was performed using the Illumina TruSeq^{TM} RNA Sample Prep Kit. Sequencing and data analysis were conducted on the Illumina NovaSeq 6000 platform at Majorbio (Shanghai Majorbio BioPharm Technology, China) using the reference genome GRCz11 (*Danio rerio*) (http://asia.ensembl.org/Danio_rerio/Info/Index). Differential expression analysis was conducted using DESeq2, with the screening threshold set to $|\log_2 FC|>=1$ and *P*-adjust<0.05.

Statistical analysis

Statistical analysis was performed using GraphPad Prism v.6.01. All data were presented as mean±standard error of the mean (SEM). Analysis of significance (*P* value) between two groups was performed using two-tailed student's *t*-tests. Analysis of significance (*P* value) among multiple groups was performed using one-way analysis of variance (ANOVA). *: $P<0.05$; **: $P<0.01$; ***: $P<0.001$.

RESULTS

Generation of *fcsk* knockout zebrafish

Expression analysis revealed that *fcsk* was expressed during various stages of early embryonic development (Supplementary Figure S1). In adult zebrafish, *fcsk* expression was markedly higher in the brain compared to other tissues, suggesting a potential role in neurodevelopment (Supplementary Figure S1). Based on these findings, we hypothesized that *fcsk* may play a crucial role in zebrafish development, particularly in the brain. To confirm this hypothesis, we generated *fcsk* knockout (*fcsk*$^{-/-}$) zebrafish using CRISPR/Cas9 technology. The target site was located in exon 3 of the *fcsk* gene (Figure 1A). Homozygous *fcsk* mutants (c.160_164delTGGGA) were identified via Sanger sequencing and restriction enzyme digestion (Figure 1B, C). The c.160_164delTGGGA mutation induced a frameshift mutation, introducing a premature stop codon (p.W54Rfs*13), which severely truncated the Fcsk protein (Figure 1B). Sequence alignment showed that 58% of amino acid residues were conserved between zebrafish Fcsk and human FCSK, and both proteins contained fucokinase, GHMP-KINASE-N, and GHMP-KINASE-C domains (Figure 1D). The mutant Fcsk protein was truncated in *fcsk*$^{-/-}$ zebrafish, retaining only a portion of the fucokinase domain (Figure 1D). Furthermore, *fcsk* mRNA levels were significantly reduced in *fcsk*$^{-/-}$ zebrafish (5 dpf) (Figure 1E).

Developmental delays and brain atrophy in *fcsk*$^{-/-}$ zebrafish

The *fcsk*$^{-/-}$ embryos exhibited pronounced epiboly delay from 6 hpf to 10 hpf, as well as developmental delays from the segmentation (12 hpf) to pharyngula periods (26 hpf) (Figure 2A). To systematically assess epiboly progression at 10 hpf, WT and *fcsk*$^{-/-}$ embryos were categorized into four classes: Class I: Completion of epiboly with tail bud formation; Class II: Completion of epiboly without tail bud formation; Class III: 85% epiboly completed; and Class IV: 60% epiboly completed. While the majority of WT embryos had completed epiboly and formed tail buds (Class I) at 10 hpf, the majority of *fcsk*$^{-/-}$ embryos remained stalled at 85% epiboly (Class III) (Figure 2B), indicating a significant developmental delay. To further investigate this phenotype, DNA content was quantitatively analyzed pre- and post-mid-blastula transition (MBT, 2.5 hpf–5.5 hpf). Results showed that *fcsk*$^{-/-}$ embryos exhibited a significant reduction in total DNA content and delayed DNA accumulation, suggesting a lower rate of cell division during pre- and post-MBT stages (Figure 2C). At 5 dpf, *fcsk*$^{-/-}$ larvae were significantly shorter than their WT counterparts (Figure 2D), which persisted into adulthood, with *fcsk*$^{-/-}$ zebrafish (4.5 mpf) being significantly shorter than WT zebrafish (Figure 2E, F). Body length measurements were conducted without considering sex-based differences (Figure 2E, F). Additionally, brain size and weight were significantly reduced in *fcsk*$^{-/-}$ adults compared to WT zebrafish (Figure 2G), further suggesting that *fcsk* is essential for both brain and body development in zebrafish.

***fcsk* knockout impairs locomotion, induces behavioral deficits, and increases seizure susceptibility in zebrafish**

Patients carrying *FCSK* mutations often present with hypotonia and seizures. To determine whether *fcsk* deficiency leads to similar impairments in zebrafish, motor and neurological functions were assessed using the light-dark stimulation test and PTZ-induced seizure assay in 6 dpf larvae (Figure 3). The light-dark stimulation test, a widely used assay for evaluating responsiveness and motor activity, was conducted over four cycles of alternating light and dark

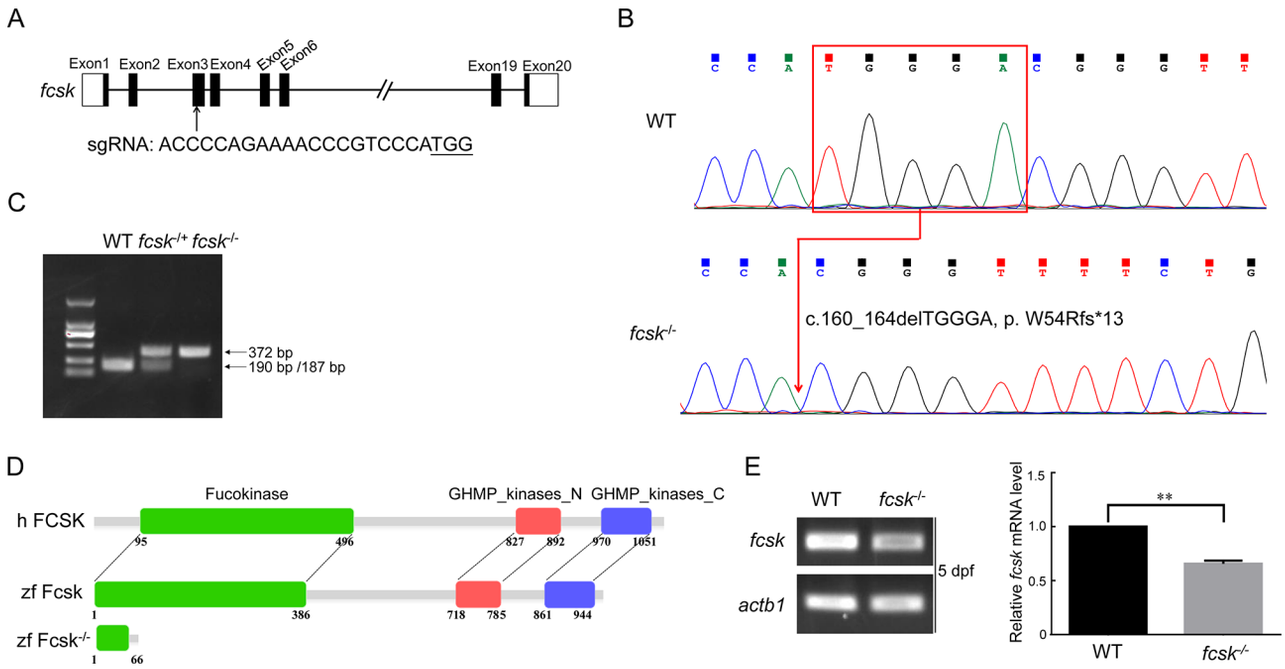

Figure 1 CRISPR/Cas9-mediated *fcsk* knockout in zebrafish

A: CRISPR/Cas9 target sites in *fcsk*. B: Sanger sequencing confirmed a five-base deletion (c.160_164delTGGGA, p.W54Rfs*13) in F_2 generation of *fcsk*$^{-/-}$ zebrafish. C: *fcsk* mutation abolished the NcoI cleavage site, preventing digestion of the PCR products in homozygous (*fcsk*$^{-/-}$) zebrafish (372 bp). In contrast, PCR products from WT zebrafish were cleaved into 190 bp and 187 bp fragments, while heterozygous (*fcsk*$^{+/-}$) zebrafish exhibited digestion of the WT allele, resulting in 372 bp, 190 bp, and 187 bp fragments. D: Protein structure of human FCSK (h FCSK), zebrafish WT Fcsk (zf Fcsk) and mutant Fcsk (zf Fcsk$^{-/-}$). E: Relative mRNA levels of *fcsk* in *fcsk*$^{-/-}$ zebrafish (5 dpf) were detected by semi-quantitative RT-PCR. dpf: Days post-fertilization. Results are presented as mean±SEM, n=3. **: P<0.01.

stimulation. Compared to WT larvae, *fcsk*$^{-/-}$ larvae exhibited a marked decrease in motor activity, with the most pronounced deficit occurring during dark phases, suggesting impaired sensorimotor responses (Figure 3A). To further assess seizure susceptibility, trajectory plots and heatmaps of larval movement were generated following PTZ exposure (Figure 3B). Compared to WT larvae, *fcsk*$^{-/-}$ larvae displayed a prolonged duration of PTZ-induced high-speed movements (>20 mm/s threshold) (Figure 3B). As prolonged high-speed movement is a hallmark of seizure-like behavior in zebrafish, these findings indicate that *fcsk*$^{-/-}$ mutants exhibit heightened seizure susceptibility (Figure 3B). Together, these results demonstrate that loss of *fcsk* impairs locomotion function, disrupts behavioral responses, and increases susceptibility to seizures in zebrafish larvae.

To determine whether *fcsk* knockout induces anxiety-like behavior in adult zebrafish, the novel tank test was conducted. The tank was divided into upper, middle, and bottom zones, and time spent in each area was tracked over a 10 min period (Figure 4A). Anxious zebrafish often exhibit escape-like or safety-seeking behaviors, leading to increased swimming distances, and preferentially remain in the bottom zone, where they perceive greater protection from potential threats (Egan et al., 2009). Results showed that *fcsk*$^{-/-}$ zebrafish (3 mpf) displayed a significant increase in total movement distance and time spent in the bottom zone, indicating a heightened anxiety phenotype (Figure 4A).

To assess the impact of *fcsk* knockout on aggression in adult zebrafish, the mirror biting test was performed (Figure 4B). Normally, zebrafish perceive their reflection as a competitor and exhibit aggressive behaviors such as prolonged engagement in the contact zone. However, *fcsk*$^{-/-}$ zebrafish (3 mpf) spent significantly less time in the contact region and more time in the far region, suggesting a marked reduction in aggressive behavior (Figure 4B).

Social behavior of adult zebrafish was evaluated using the social preference and shoaling tests (Figure 4C, D). In the social preference test, total movement distance was significantly reduced in *fcsk*$^{-/-}$ zebrafish (3 mpf), and no significant difference in time spent in the left and right areas was observed, indicating impaired sociability (Figure 4C). Similarly, in the shoaling test, *fcsk*$^{-/-}$ zebrafish (3 mpf) exhibited increased inter-individual distances and reduced clustering behavior, suggesting attenuated social preference and impaired group coordination (Figure 4D). Cognitive function was assessed using the modified T-maze test, which evaluates learning and spatial memory retention. In this test, zebrafish learn to avoid the punishment arm, where a mild aversive stimulus is applied. Results showed that *fcsk*$^{-/-}$ zebrafish (3 mpf) exhibited a significantly shorter latency to enter the punishment arm, demonstrating deficits in learning and memory (Figure 4E).

Collectively, these findings indicate that *fcsk*$^{-/-}$ zebrafish display profound neurobehavioral abnormalities, characterized by increased anxiety, attenuated aggressiveness, impaired social preference, and deficits in learning and memory.

fcsk$^{-/-}$ zebrafish exhibit increased midbrain-hindbrain boundary (MHB) apoptosis, decreased fucosylated protein levels, and reduced *pofut2* expression

Structural brain abnormalities, particularly corpus callosum dysplasia, have been reported in the majority of *FCSK*-deficient patients (4/5 cases) (Al Tuwaijri et al., 2023; Manoochehri et al., 2022; Ng et al., 2018a; Özgün & Şahin, 2022). To investigate whether *fcsk* loss-of-function affects zebrafish neurodevelopment, AO staining was used to assess

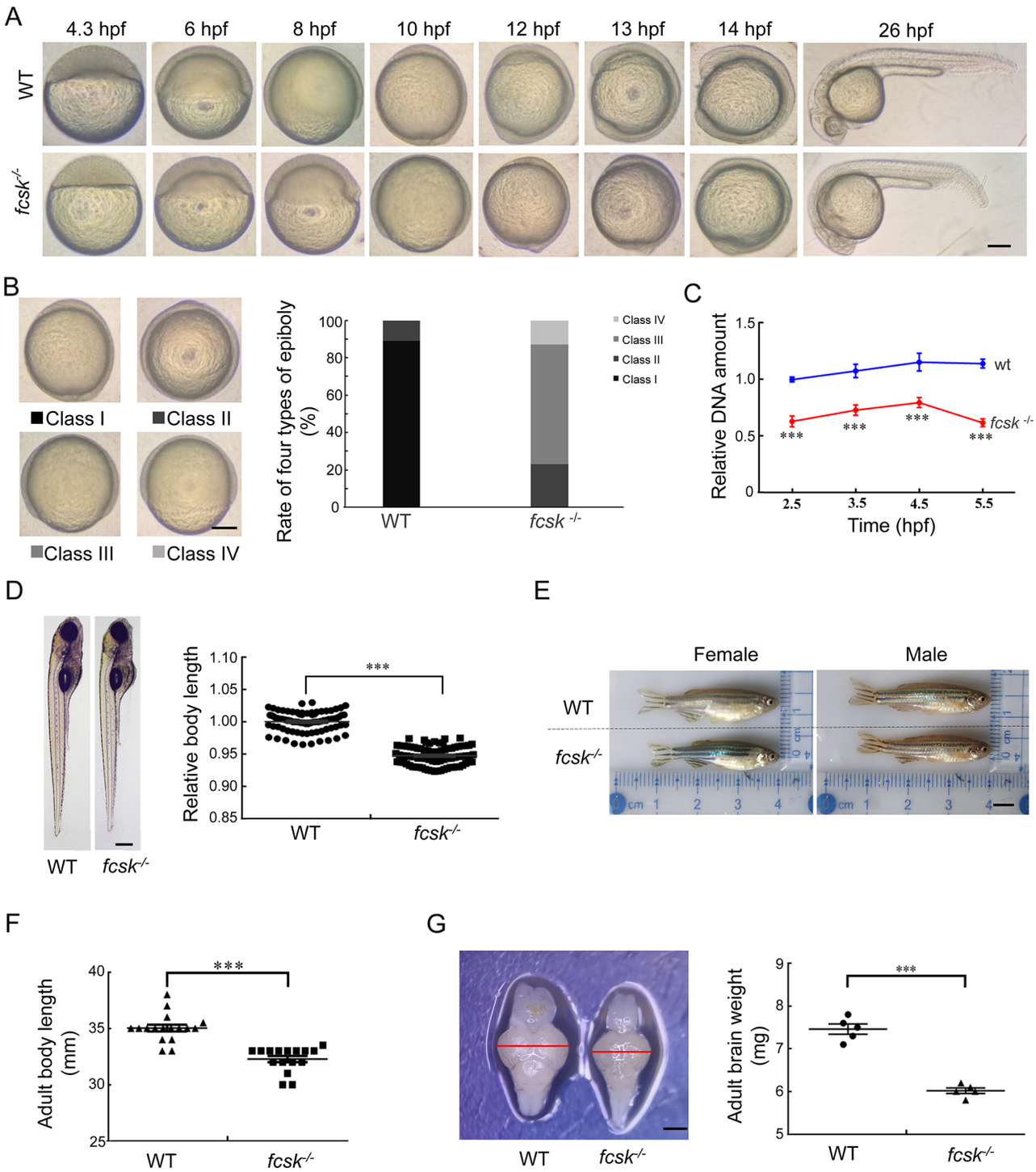

Figure 2 Developmental retardation and brain atrophy in *fcsk*$^{-/-}$ zebrafish

A: Representative images showing developmental delay in *fcsk*$^{-/-}$ embryos from 4.3 hpf to 26 hpf. hpf: Hours post-fertilization. Scale bar: 200 μm. B: Classification of epiboly progression at 10 hpf into four stages: Class I (epiboly completed, tail bud formed), Class II (epiboly completed, no tail bud formed), Class III (approximately 85% epiboly), and Class IV (approximately 60% epiboly). The proportion of these types was quantified in WT and *fcsk*$^{-/-}$ embryos (100 per group). Scale bar: 200 μm. C: Quantitative DNA content analysis in WT and *fcsk*$^{-/-}$ embryos pre- and post-MBT (2.5–5.5 hpf). Thirty embryos were collected at each time point under identical culture conditions. *n*=3. D: Body length comparison of WT and *fcsk*$^{-/-}$ larvae (5 dpf, 80 larvae per group). Scale bar: 200 μm. E: Body length comparison of WT and *fcsk*$^{-/-}$ adult zebrafish (4.5 mpf, female and male). mpf: Months post-fertilization. Scale bar: 0.5 cm. F: Statistical analysis of adult body length in 17 WT and 16 *fcsk*$^{-/-}$ zebrafish. G: Brain size (left) and weight (right) of *fcsk*$^{-/-}$ zebrafish (4.5 mpf). *n*=5. Scale bar: 200 μm. Mean±SEM. ***: *P*<0.001.

apoptosis in *fcsk*$^{-/-}$ larvae. Results showed a significant increase in apoptotic cell at the MHB in *fcsk*$^{-/-}$ larvae compared to WT controls (Figure 5A).

To evaluate the impact of *fcsk* deficiency on fucosylation, AAL blot analysis was performed. Results revealed a significant reduction in total fucosylated proteins in *fcsk*$^{-/-}$ zebrafish compared to WT controls (Figure 5B). Furthermore, the expression levels of genes involved in the GDP-fucose

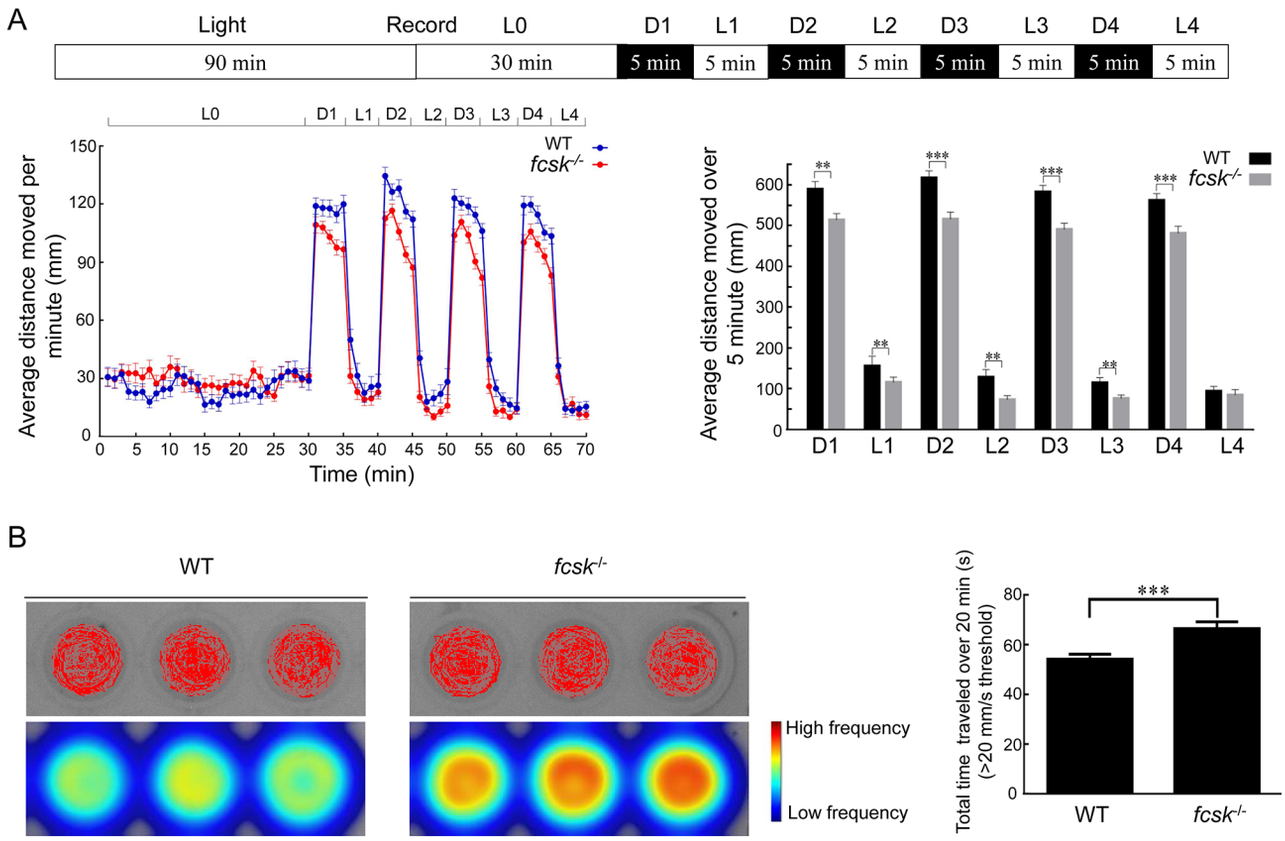

Figure 3 Light-dark stimulation and PTZ induction seizure susceptibility in zebrafish larvae

A: Experimental protocol for light-dark stimulation test. Average distance traveled by *fcsk*$^{-/-}$ larvae (6 dpf) under light and dark stimuli. *n*=48 per genotype. L: Light; D: Dark. B: Representative trajectory plots and heatmaps of PTZ-induced larvae (6 dpf), and duration of high-speed movements (>20 mm/s threshold) was significantly increased in *fcsk*$^{-/-}$ larvae compared to WT controls. *n*=48 per genotype. Mean±SEM. **: *P*<0.01; ***: *P*<0.001.

salvage synthesis pathway (*fpgt*, *slc35c2*, *pofut1*, and *pofut2*) were detected by semi-quantitative RT-PCR, with results showing a significant decrease in *pofut2* expression in *fcsk*$^{-/-}$ zebrafish (Figure 5C).

Taken together, these findings indicate that developmental delay, neuroanatomical abnormalities, and behavioral deficits in *fcsk*$^{-/-}$ zebrafish may be related to the increased apoptosis at the MHB and decreased levels of fucosylated proteins.

GDP-L-fucose and GFP-tagged human *FCSK* plasmid rescue developmental delays and restore fucosylation in *fcsk*$^{-/-}$ zebrafish

Given that *fcsk* functions upstream in the fucosylation salvage pathway, we speculated that exogenous supplementation with GDP-L-fucose, a downstream product, may effectively alleviate developmental defects in *fcsk*$^{-/-}$ zebrafish. Indeed, injection of GDP-L-fucose led to a significant elevation in total protein fucosylation levels and accelerated early embryonic development in *fcsk*$^{-/-}$ zebrafish, indicating a partial rescue of *fcsk* deficiency (Figure 6A, B). Furthermore, given the high sequence homology between human *FCSK* and zebrafish *fcsk*, we speculated that human *FCSK* may effectively alleviate the developmental defects and protein fucosylation levels observed in *fcsk*$^{-/-}$ zebrafish. Results showed that injection of a GFP-tagged human *FCSK* expression plasmid into *fcsk*$^{-/-}$ zebrafish resulted in a marked improvement in early developmental progression and a restoration of protein fucosylation levels (Figure 6C, D).

RNA-seq analysis of WT and *fcsk*$^{-/-}$ zebrafish

To further explore the molecular mechanisms underlying *fcsk* deficiency-induced neurodevelopmental disorders, RNA-seq analysis was performed on WT and *fcsk*$^{-/-}$ zebrafish. Differential gene expression analysis identified 750 down-regulated genes and 580 up-regulated genes, indicating widespread transcriptional dysregulation in *fcsk*$^{-/-}$ mutants (Figure 7A). Among the dysregulated genes *st8sia7.1* and *st8sia6*, which encode ST8 alpha-N-acetyl-neuraminide alpha-2,8-sialyltransferase, were significantly down-regulated, indicating impaired glycosylation in *fcsk*$^{-/-}$ zebrafish (Figure 7B, C). These enzymes play key roles in N-glycan processing, oligosaccharide metabolism, and protein glycosylation (Shih et al., 2023). Gene enrichment and RT-qPCR analysis confirmed the suppression of *st8sia7.1* and *st8sia6* expression, suggesting that *fcsk* deficiency disrupts glycosylation homeostasis in zebrafish.

To investigate the relationship between *fcsk* deficiency and apoptosis, apoptosis-related genes were analyzed. *zgc-162184*, *pmaip1*, and *capn2l* are known to facilitate apoptosis, while *akt2l*, *pik3r3b*, and *gadd45ga* are known to inhibit apoptosis (Antonio et al., 2023; Huang et al., 2023; Shin et al., 2021; Wang et al., 2020; Zhao et al., 2014). Enrichment analysis and RT-qPCR indicated that pro-apoptotic genes *zgc-162184*, *pmaip1*, and *capn2l* were significantly up-regulated, while anti-apoptotic genes *akt2l*, *pik3r3b*, and *gadd45ga* were significantly down-regulated (Figure 7D, E).

Differentially expressed genes associated with neurological

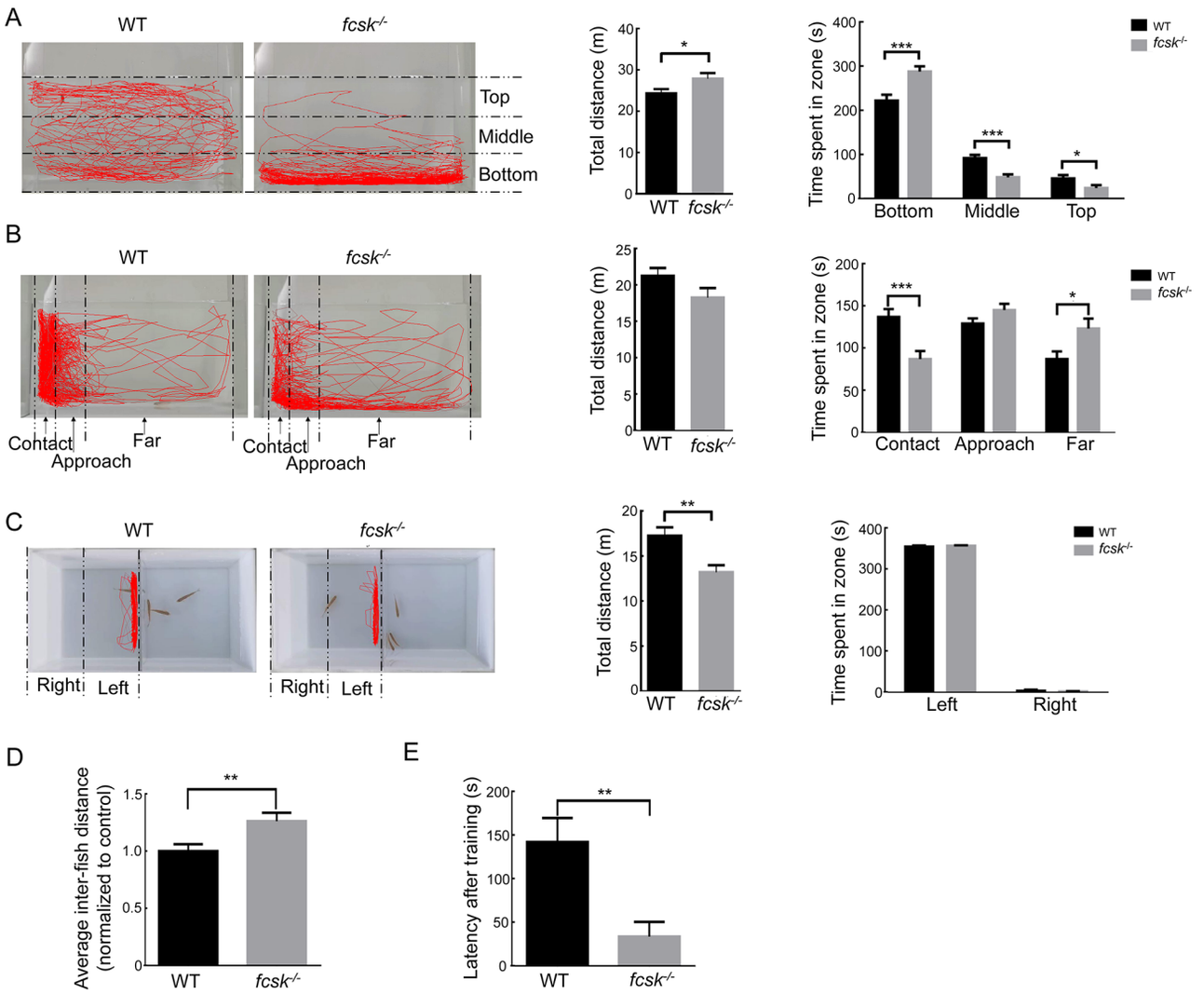

Figure 4 Behavioral assessments of adult zebrafish

A: Novel tank test. Representative trajectory plots (left) and quantitative analysis (right) showing total movement distance and time spent in bottom, middle, and top regions in WT and *fcsk*$^{-/-}$ zebrafish (3 mpf, *n*=31 per group). B: Mirror biting test. Representative trajectory plots (left) and quantitative analysis (right) of total movement distance and time spent in contact, approach, and far zones in WT (*n*=23) and *fcsk*$^{-/-}$ (*n*=21) zebrafish (3 mpf). C: Social preference test. Representative trajectory plots (left) and quantitative analysis (right) showing a significant reduction in total movement distance in *fcsk*$^{-/-}$ zebrafish (3 mpf, *n*=20 per group), with no significant difference observed in time spent in left and right regions. D: Shoaling test. Average inter-fish distance was significantly increased in *fcsk*$^{-/-}$ zebrafish (3 mpf, *n*=24 per group), indicating reduced social cohesion. E: Modified T-maze test. *fcsk*$^{-/-}$ zebrafish (3 mpf) exhibited a significantly shorter latency to enter the punishment arm, suggesting impaired learning and memory function (*n*=24 per group).

functions were subjected to KEGG pathway enrichment analysis (Figure 7F), revealing significant alterations in multiple neurodegenerative disease pathways, including Parkinson's disease, Alzheimer's disease, Huntington's disease, spinocerebellar ataxia, and amyotrophic lateral sclerosis (ALS) (Figure 7F). Among the dysregulated genes, *FUS*, an RNA-binding protein involved in RNA metabolism, was significantly down-regulated (Figure 7G, H). *FUS* mutations are known to cause ALS, a progressive neurodegenerative disorder characterized by motor neuron loss and muscle weakness (Vance et al., 2009). Enrichment analysis of neurodegeneration-related genes, along with RT-qPCR validation, confirmed the reduced expression of *fus* (Figure 7G, H).

DISCUSSION

In this study, we established the first *fcsk* knockout animal model using CRISPR/Cas9 genome-editing technology. Notably, *fcsk*$^{-/-}$ zebrafish exhibited developmental delays from embryogenesis to adulthood, increased seizure susceptibility, and profound neurobehavioral abnormalities. To date, four studies have reported one compound heterozygous mutation (c.667T>C, c.2047C>T) and five homozygous mutations (c.2980A>C, c.993_1011del, c.379C>A, c.394G>C, and c.3013G>C) in the human *FCSK* gene (Al Tuwaijri et al., 2023; Manoochehri et al., 2022; Ng et al., 2018a; Özgün & Şahin, 2022). Patients carrying these mutations present with developmental delay, hypotonia, encephalopathy, and ocular abnormalities (Al Tuwaijri et al., 2023; Manoochehri et al., 2022; Ng et al., 2018a; Özgün & Şahin, 2022), aligning closely with the phenotypic spectrum observed in *fcsk*$^{-/-}$ zebrafish, including delayed development, impaired locomotion, brain atrophy, seizure susceptibility, heightened anxiety, reduced aggression, impaired social preference, and deficits in

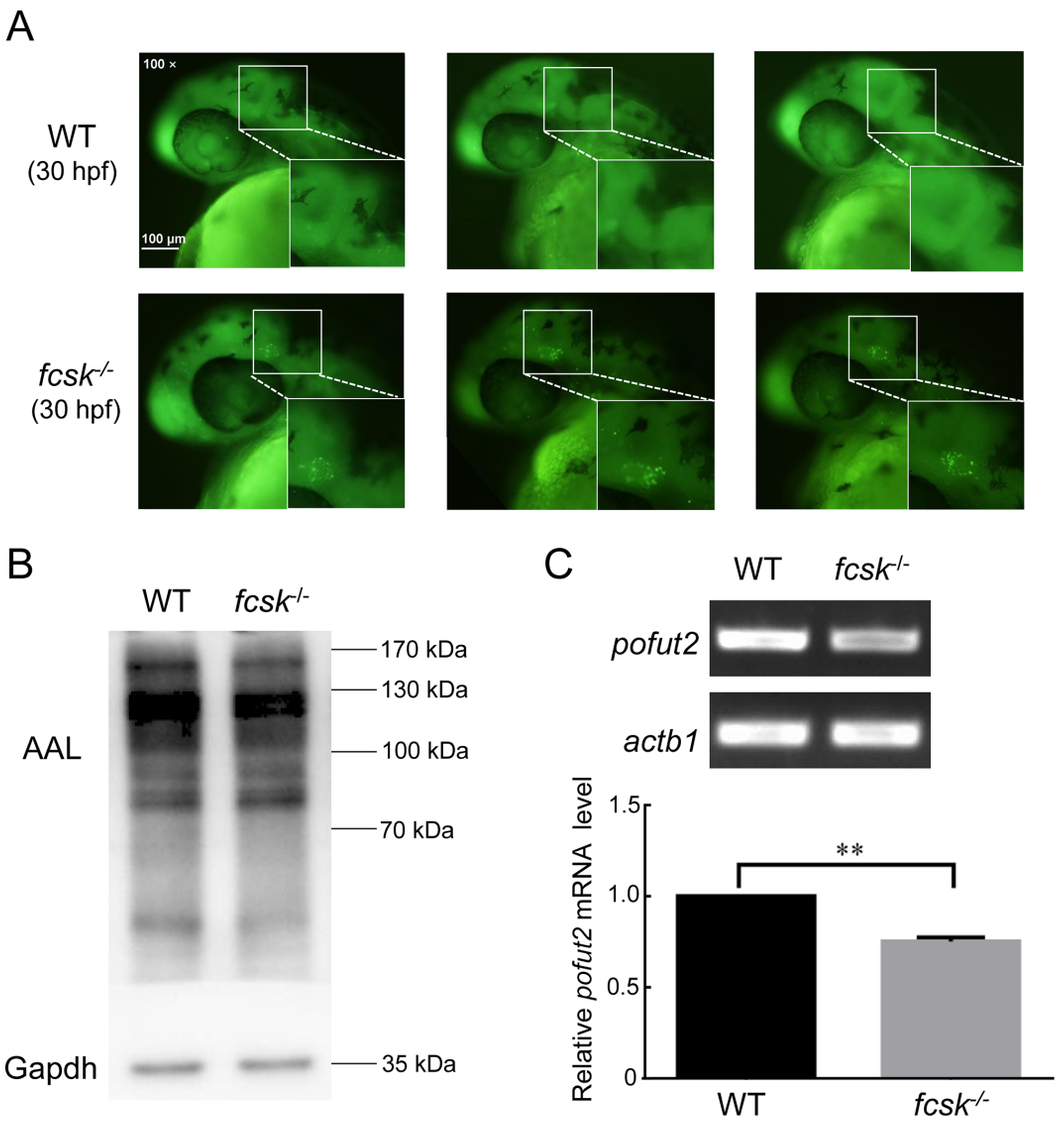

Figure 5 Increased apoptosis in midbrain-hindbrain boundary and decreased expression of fucosylated proteins and *pofut2* in *fcsk*$^{-/-}$ zebrafish

A: Representative acridine orange (AO) staining results of WT (*n*=22) and *fcsk*$^{-/-}$ (*n*=21) larvae (30 hpf). White box: Mid-hindbrain boundary. Enlarged images of white boxed areas are shown in lower right corner. Scale bar: 100 μm. B: Western and lectin blot analyses of WT and *fcsk*$^{-/-}$ zebrafish at 5 dpf. Gapdh was used as an internal control. *n*=20 larvae (5 dpf) per genotype. AAL: *Aleuria aurantia* lectin. *n*=3. C: Agarose gel electrophoresis (upper) and statistical analysis (lower) of semi-quantitative RT-PCR for *pofut2* expression in WT and *fcsk*$^{-/-}$ zebrafish (5 dpf). *n*=3. Mean±SEM. **: *P*<0.01.

memory.

The MHB is a crucial signaling center that orchestrates neuronal migration, ventricular partitioning, and cerebellar development (Kesavan et al., 2020). Our results showed that *fcsk*$^{-/-}$ zebrafish exhibited increased apoptosis within the MHB, potentially disrupting midbrain and cerebellar formation and contributing to brain atrophy. In addition, RNA-seq analysis indicated that pro-apoptotic gene expression was up-regulated, while anti-apoptotic gene expression was down-regulated, confirming the occurrence of apoptosis in *fcsk*$^{-/-}$ zebrafish.

Total GDP-fucose levels are significantly reduced in skin fibroblasts derived from individuals with *FCSK* mutations (Ng et al., 2018a). Similarly, *fcsk*$^{-/-}$ zebrafish exhibited a marked reduction in fucosylated protein levels. *Pofut2* is essential for normal limb skeletal development, with *Pofut2* knockout mice exhibiting early embryonic death (Benz et al., 2016; Neupane et al., 2022). Our results indicated that *fcsk*$^{-/-}$ zebrafish exhibited reduced *pofut2* expression, which may impair skeletal development and contribute to their reduced body length.

Fucosylated proteins play a crucial role in embryonic development, especially in neuronal tissue (Hüllen et al., 2021). The significant reduction in fucosylated protein levels observed in *fcsk*$^{-/-}$ zebrafish likely contributed to their developmental delays and abnormal behavior. Mutations in *FUS* are implicated in the development of ALS, clinically characterized by motor neuron degeneration (Corrado et al., 2010). Here, RNA-seq analysis revealed a marked down-regulation of *fus* (the zebrafish homolog of human *FUS*) in *fcsk*$^{-/-}$ zebrafish, suggesting a potential mechanistic link between *fcsk* deficiency and impaired motor and cognitive function in zebrafish. Fucosylated lipids are also integral to cell adhesion, spermatogenesis, and early embryonic

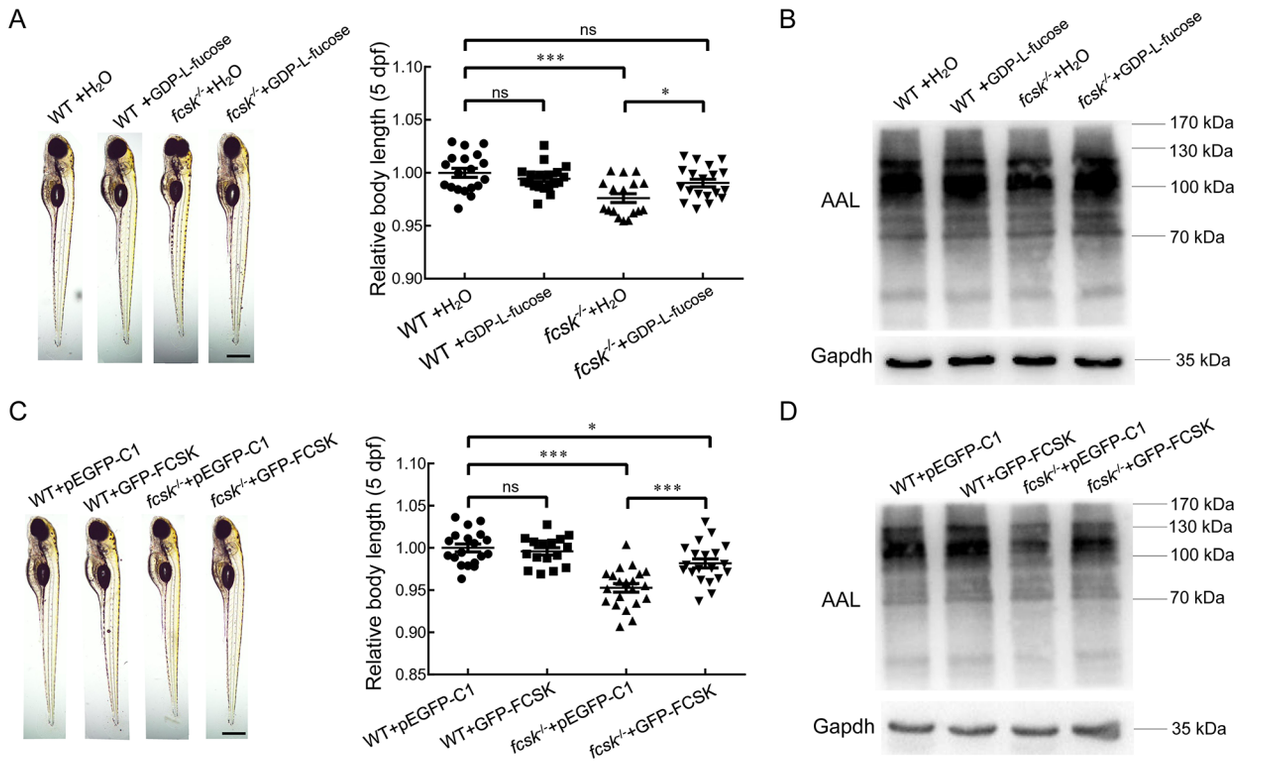

Figure 6 GDP-L-fucose and GFP-tagged human *FCSK* rescue early development and fucosylated protein levels in *fcsk*$^{-/-}$ zebrafish

A: Body length and statistical analysis of WT (injected with H_2O), WT (injected with GDP-L-fucose), *fcsk*$^{-/-}$ (injected with H_2O), and *fcsk*$^{-/-}$ (injected with GDP-L-fucose) zebrafish (5 dpf, *n*=24). Scale bar: 200 μm. B: Western and lectin blot analyses of WT (injected with H_2O), WT (injected with GDP-L-fucose), *fcsk*$^{-/-}$ (injected with H_2O), and *fcsk*$^{-/-}$ (injected with GDP-L-fucose) zebrafish (48 hpf). C: Body length and statistical analysis of WT (injected with pEGFP-C1), WT (injected with GFP-tagged human *FCSK*), *fcsk*$^{-/-}$ (injected with pEGFP-C1), and *fcsk*$^{-/-}$ (injected with GFP-tagged human *FCSK*) zebrafish (5 dpf, *n*=19). Scale bar: 200 μm. D: Western and lectin blot analyses of WT (injected with pEGFP-C1), WT (injected with GFP-tagged human *FCSK*), *fcsk*$^{-/-}$ (injected with pEGFP-C1), and *fcsk*$^{-/-}$ (injected with GFP-tagged human *FCSK*) zebrafish (72 hpf). Mean±SEM. ns: Not significant; *: *P*<0.05; ***: *P*<0.001.

development (Iwamori et al., 2020). Disruption of *fcsk* function may also impair the synthesis of fucosylated lipids, further compromising early embryonic development and contributing to the observed growth deficits in zebrafish.

Currently, no effective pharmacological treatments are available for patients with fucosylation deficiencies. Vitamin B12 supplementation has shown limited therapeutic benefit in individuals with *FCSK*-CDG, failing to significantly improve clinical symptoms (Ng et al., 2018a). Conversely, L-fucose supplementation has exhibited efficacy in alleviating immune-related symptoms in most *SLC35C1*-CDG patients (Hüllen et al., 2021). However, its therapeutic efficacy in *FCSK*-deficient patients remains unclear. In this study, we demonstrated that both GDP-L-fucose supplementation and human *FCSK* gene expression effectively rescued early developmental progression and protein fucosylation levels in *fcsk*$^{-/-}$ zebrafish. These findings suggest that *fcsk*$^{-/-}$ zebrafish can provide a valuable platform for drug screening and therapeutic exploration for *FCSK*-related disorders.

In conclusion, we established the first vertebrate model of *FCSK*-CDG by generating *fcsk*$^{-/-}$ zebrafish, which displayed developmental delay, locomotor deficits, impaired social behavior and memory, increased seizure susceptibility, and increased anxiety-like behavior. Transcriptomic analysis revealed significant dysregulation of genes involved in glycosylation, apoptosis, and neurodegenerative pathways, shedding light on the molecular mechanisms underlying *FCSK* deficiency. These findings deepen our understanding of the pathophysiology of CDG and provide preclinical evidence supporting GDP-L-fucose as a potential therapeutic intervention for *FCSK* deficiency in humans.

DATA AVAILABILITY

The transcriptomic data were submitted to the NCBI sequence read archive under BioProjectID PRJNA1191638, GSA database under accession number CRA020563, and Science Data Bank under doi: 10.57760/sciencedb.j00139.00126.

SUPPLEMENTARY DATA

Supplementary data to this article can be found online.

COMPETING INTERESTS

The authors declare that they have no competing interests.

AUTHORS' CONTRIBUTIONS

X.Q.Z. conceived and designed the study. Z.X.L. prepared the draft manuscript. Z.X.L., T.T.Z., and H.H.L. acquired and analyzed the data. X.Q.Z. and H.B.J. revised and finalized the manuscript. All authors read and approved the final version of the manuscript.

ACKNOWLEDGMENTS

We thank the Research Core Facilities for Life Science (HUST).

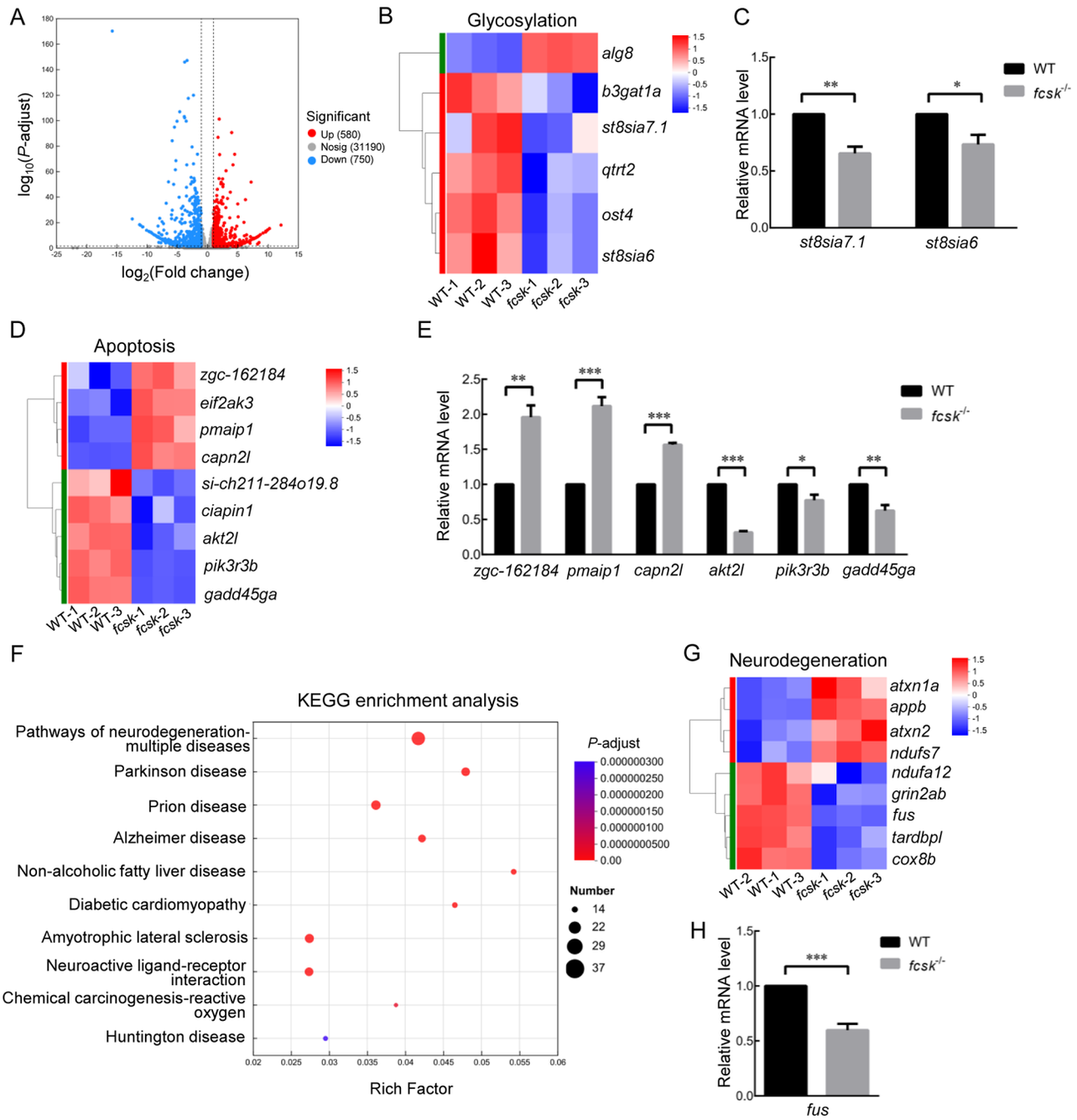

Figure 7 RNA-seq analysis of WT and *fcsk*$^{-/-}$ zebrafish

A: Volcano plot of differentially expressed genes (DEGs) between WT and *fcsk*$^{-/-}$ zebrafish. Blue represents down-regulated genes (750), red represents up-regulated genes (580), gray represents genes with no significant difference. B: Clustering heatmap of glycosylation-related DEGs. C: mRNA levels of glycosylation-related DEGs detected by RT-qPCR (n=3). D: Clustering heatmap of apoptosis-related DEGs. E: mRNA levels of apoptosis-related DEGs detected by RT-qPCR (n=3). F: KEGG analysis of DEGs related to the nervous system. G: Clustering heatmap of DEGs homologous to human neurodegenerative disease-related genes. H: mRNA levels of neurodegeneration-related DEGs detected by RT-qPCR (n=3). Mean±SEM. *: P<0.05; **: P<0.01; ***: P<0.001.

REFERENCES

Al Tuwaijri A, Alyafee Y, Umair M, et al. 2023. Congenital disorder of glycosylation with defective fucosylation 2 (*FCSK* gene defect): the third report in the literature with a mild phenotype. *Molecular Genetics & Genomic Medicine*, **11**(4): e2117.

Antonio LGL, Meola J, de Sá Rosa-e-Silva ACJ, et al. 2023. Altered differential expression of genes and microRNAs related to adhesion and apoptosis pathways in patients with different phenotypes of endometriosis. *International Journal of Molecular Sciences*, **24**(5): 4434.

Benz BA, Nandadasa S, Takeuchi M, et al. 2016. Genetic and biochemical evidence that gastrulation defects in *Pofut2* mutants result from defects in ADAMTS9 secretion. *Developmental Biology*, **416**(1): 111–122.

Corrado L, Del Bo R, Castellotti B, et al. 2010. Mutations of *FUS* gene in sporadic amyotrophic lateral sclerosis. *Journal of Medical Genetics*, **47**(3): 190–194.

Egan RJ, Bergner CL, Hart PC, et al. 2009. Understanding behavioral and physiological phenotypes of stress and anxiety in zebrafish. *Behavioural Brain Research*, **205**(1): 38–44.

Feichtinger RG, Hüllen A, Koller A, et al. 2021. A spoonful of L-fucose-an efficient therapy for GFUS-CDG, a new glycosylation disorder. *EMBO Molecular Medicine*, **13**(9): e14332.

Fowler G, French DV, Rose A, et al. 2021. Protein fucosylation is required for Notch dependent vascular integrity in zebrafish. *Developmental Biology*, **480**: 62–68.

Hayashiji N, Kawahara G, Xu X, et al. 2022. α-1, 6-Fucosyltransferase is essential for myogenesis in zebrafish. *Cells*, **12**(1): 144.

Huang B, Wu GZ, Peng CX, et al. 2023. miR-126 regulates the proliferation, migration, invasion, and apoptosis of non-small lung cancer cells via AKT2/HK2 axis. *IUBMB Life*, **75**(3): 186–195.

Hüllen A, Falkenstein K, Weigel C, et al. 2021. Congenital disorders of glycosylation with defective fucosylation. *Journal of Inherited Metabolic Disease*, **44**(6): 1441–1452.

Iwamori M, Adachi S, Lin B, et al. 2020. Spermatogenesis-associated changes of fucosylated glycolipids in murine testis. *Human Cell*, **33**(1): 23–28.

Kesavan G, Machate A, Hans S, et al. 2020. Cell-fate plasticity, adhesion and cell sorting complementarily establish a sharp midbrain-hindbrain boundary. *Development*, **147**(11): dev186882.

Li M, Cheng RH, Liang JY, et al. 2013. Mutations in *POFUT1*, encoding protein O-fucosyltransferase 1, cause generalized Dowling-Degos disease. *The American Journal of Human Genetics*, **92**(6): 895–903.

Liu CX, Li CY, Hu CC, et al. 2018. CRISPR/Cas9-induced *shank3b* mutant zebrafish display autism-like behaviors. *Molecular Autism*, **9**: 23.

Manoochehri J, Kamal N, Khamirani HJ, et al. 2022. A combination of two novels homozygous FCSK variants cause disorder of glycosylation with defective fucosylation: new patient and literature review. *European Journal of Medical Genetics*, **65**(8): 104535.

Neupane S, Berardinelli SJ, Cameron DC, et al. 2022. *O*-fucosylation of thrombospondin type 1 repeats is essential for ECM remodeling and signaling during bone development. *Matrix Biology*, **107**: 77–96.

Ng BG, Freeze HH. 2018. Perspectives on glycosylation and its congenital disorders. *Trends in Genetics*, **34**(6): 466–476.

Ng BG, Rosenfeld JA, Emrick L, et al. 2018a. Pathogenic variants in fucokinase cause a congenital disorder of glycosylation. *The American Journal of Human Genetics*, **103**(6): 1030–1037.

Ng BG, Xu GG, Chandy N, et al. 2018b. Biallelic mutations in *FUT8* cause a congenital disorder of glycosylation with defective fucosylation. *The American Journal of Human Genetics*, **102**(1): 188–195.

Ngoc Hieu BT, Ngoc Anh NT, Audira G, et al. 2020. Development of a modified three-day T-maze protocol for evaluating learning and memory capacity of adult zebrafish. *International Journal of Molecular Sciences*, **21**(4): 1464.

Ondruskova N, Cechova A, Hansikova H, et al. 2021. Congenital disorders of glycosylation: still "hot" in 2020. *Biochimica et Biophysica Acta (BBA)-General Subjects*, **1865**(1): 129751.

Özgün N, Şahin Y. 2022. A case with congenital disorder of glycosylation with defective fucosylation 2 and new mutation in FUK gene. *Brain & Development*, **44**(3): 239–243.

Raymond J, Chanin S, Stewart AM, et al. 2012. Assessing habituation phenotypes in adult zebrafish: intra- and inter-trial habituation in the novel tank test. *In*: Kalueff AV, Stewart AM. Zebrafish Protocols for Neurobehavioral Research. Totowa: Humana Press, 273–285.

Shih PC, Chen HP, Hsu CC, et al. 2023. Long-term DEHP/MEHP exposure promotes colorectal cancer stemness associated with glycosylation alterations. *Environmental Pollution*, **327**: 121476.

Shin GT, Park JE, Lee MJ. 2021. MAGEH1 interacts with GADD45G and induces renal tubular cell apoptosis. *PLoS One*, **16**(11): e0260135.

Smith PL, Myers JT, Rogers CE, et al. 2002. Conditional control of selectin ligand expression and global fucosylation events in mice with a targeted mutation at the FX locus. *The Journal of Cell Biology*, **158**(4): 801–815.

Taubenschmid J, Stadlmann J, Jost M, et al. 2017. A vital sugar code for ricin toxicity. *Cell Research*, **27**(11): 1351–1364.

Vance C, Rogelj B, Hortobagyi T, et al. 2009. Mutations in FUS, an RNA processing protein, cause familial amyotrophic lateral sclerosis type 6. *Science*, **323**(5918): 1208–1211.

Wang WT, Huang ZP, Sui S, et al. 2020. microRNA-1236 promotes chondrocyte apoptosis in osteoarthritis via direct suppression of PIK3R3. *Life Sciences*, **253**: 117694.

Wang XC, Inoue S, Gu JG, et al. 2005. Dysregulation of TGF-β1 receptor activation leads to abnormal lung development and emphysema-like phenotype in core fucose-deficient mice. *Proceedings of the National Academy of Sciences of the United States of America*, **102**(44): 15791–15796.

Yakubenia S, Frommhold D, Schölch D, et al. 2008. Leukocyte trafficking in a mouse model for leukocyte adhesion deficiency II/congenital disorder of glycosylation IIc. *Blood*, **112**(4): 1472–1481.

Zhao BS, Wang X, Beadell AV, et al. 2017. m^6A-dependent maternal mRNA clearance facilitates zebrafish maternal-to-zygotic transition. *Nature*, **542**(7642): 475–478.

Zhao XF, Liu XG, Su L. 2014. Parthenolide induces apoptosis via TNFRSF10B and PMAIP1 pathways in human lung cancer cells. *Journal of Experimental & Clinical Cancer Research*, **33**(1): 3.